Fabric anisotropy & DEM informed two-surface hyperplasticity: constitutive formulation, asymptotic states & experimental validation

W.M. Coombs
School of Engineering & Computing Sciences,
Durham University, UK

R.S. Crouch
School of Engineering and Mathematical Sciences & School of Informatics,
City University London, UK.

ABSTRACT: In geotechnical analysis continuum idealisations of the bulk material still provide the most appropriate approach for engineers designing large-scale structures. In this area, the most successful framework for describing the behaviour of soils is Critical State (CS) soil mechanics. However, the findings from discrete element method (DEM) analysis, such as the uniqueness of the CS, can provide invaluable information in the development such models. This paper details the key concepts behind a two-surface hyperplasticity model (**?**) whose development was informed by recent DEM findings on the uniqueness of the CS. Asymptotic states of the model will be confirmed and the DEM-continuum-experimental loop will be closed through comparison of the developed model with experimental data on coarse-grained particulate media. This will demonstrate, that providing the previous stress history is accounted for, the proposed model is suitable for a variety of particulate media.

1 INTRODUCTION

This paper presents the constitutive formulation of a two-surface hyperplasticity model whose development was informed by recent discrete element method (DEM) findings on the uniqueness of the Critical State (CS). These recent findings, and their implications on the continuum plasticity formulations, are explored in a companion paper published in the same conference proceedings.

The layout of the paper is as follows. After this introduction, Section 2 presents the constitutive formulation of the two-surface anisotropic model, including: (i) elastic free-energy, (ii) dissipation, (iii) Lode angle dependency, (iv) isotropic hardening, (v) anisotropic shearing and (vi) inner surface translation. The asymptotic states of the model are explored in Section 3 and the model is validated against experimental data in Section 4. Finally observations are drawn in Section 5.

In this paper compressive stresses are taken as positive and the deviatoric stress measure, q, is defined as $q = \sqrt{s_{ij}s_{ij}}$ where $s_{ij} = \sigma_{ij} - p\delta_{ij}$ and $p = \sigma_{ii}/3$. σ_{ij} and δ_{ij} are the Cauchy stress and Kronecker delta tensors, respectively. It is important to note that this measure of deviatoric stress is not equal to the difference between the cell pressure, σ_3, and the axial stress, σ_1, in a triaxial apparatus, instead $q = \sqrt{2/3}(\sigma_1 - \sigma_3)$..

2 CONSTITUTIVE FORMULATION

2.1 *Elastic free-energy*

Here we use an elastic free energy function that provides pressure sensitive bulk and shear moduli (**?**)

$$\Psi_1 = \kappa p_r \exp\big(\Omega\big) + G\gamma^{\mathrm{e}}_{ij}\gamma^{\mathrm{e}}_{ij}, \tag{1}$$

where $\Omega = (\varepsilon^{\mathrm{e}}_v - \varepsilon^{\mathrm{e}}_{v0})/\kappa$ and G is the constant shear modulus. The elastic strain measures are given by $\varepsilon^{\mathrm{e}}_v = \varepsilon^{\mathrm{e}}_{ii}$ and $\gamma^{\mathrm{e}}_{ij} = \varepsilon^{\mathrm{e}}_{ij} - \varepsilon^{\mathrm{e}}_v\delta_{ij}/3$, where δ_{ij} is the Kronecker delta tensor. κ is the bi-logarithmic elastic compressibility index (the gradient of the drained unloading line in the bi-logarithmic void ratio versus hydrostatic pressure plane), p_r is the reference pressure and $\varepsilon^{\mathrm{e}}_{v0}$ is the elastic volumetric strain at that reference pressure. Taking the partial derivative of (**??**) with respect to the elastic strain, the Cauchy stress is given by

$$\sigma_{ij} = p_r \exp\big(\Omega\big)\delta_{ij} + 2G\gamma^{\mathrm{e}}_{ij}. \tag{2}$$

Taking the second derivative of the free energy function with respect to elastic strain, the non-linear elastic stiffness matrix subsequently follows as

$$D^{\mathrm{e}}_{ijkl} = \left(\frac{p_r \exp(\Omega)}{\kappa} - \frac{2G}{3}\right)\delta_{ij}\delta_{kl} + 2G\big(I_{ijkl}\big) \qquad (3)$$

where I_{ijkl} is a fourth order identity tensor.

2.2 *Dissipation*

The rate of dissipation function for the inner surface of the two-surface anisotropic model can be expressed as

$$\dot{\Phi} = \sqrt{(\dot{\varepsilon}^{\mathrm{p}}_v + \beta_{ij}\dot{\gamma}^{\mathrm{p}}_{ij})^2 A_f^2 + (\dot{\varepsilon}^{\mathrm{p}}_\gamma B_f)^2} \qquad (4)$$

with $\varepsilon^{\mathrm{p}}_v = \varepsilon^{\mathrm{p}}_{ii}$, $\gamma^{\mathrm{p}}_{ij} = \varepsilon^{\mathrm{p}}_{ij} - (\varepsilon^{\mathrm{p}}_v/3)\delta_{ij}$ and $\varepsilon^{\mathrm{p}}_\gamma = \sqrt{\gamma^{\mathrm{p}}_{ij}\gamma^{\mathrm{p}}_{ij}}$, where β_{ij} accounts for the coupling between volumetric and deviatoric plastic straining. Following the standard procedure, as given by **?**), we obtain the inner anisotropic yield surface in true stress space as

$$f = (p - p^\chi)^2 B_f^2 + s^\beta_{ij} s^\beta_{ij} A_f^2 - A_f^2 B_f^2 = 0, \qquad (5)$$

where the *local deviatoric stress* is given by $s^\beta_{ij} = s_{ij} - s^\chi_{ij} - (p - p^\chi)\beta_{ij}$. As shown in Figure **??**, $p^\chi = \sigma^\chi_{ii}/3$ and $s^\chi_{ij} = \sigma^\chi_{ij} - p^\chi\delta_{ij}$ are the hydrostatic and deviatoric components of the centre of the inner yield surface, σ^χ_{ij}. The stress-like quantities controlling the shape of the yield envelope are given by

$$\begin{aligned} A_f &= (1-\gamma)(p-p^\chi) + (2-\gamma)\gamma R p_c/2 \quad \text{and} \\ B_f &= \bar{\rho}(\theta) M\big((1-\alpha)(p-p^\chi) + \gamma R p_c/2\big). \end{aligned} \qquad (6)$$

p_c and M control the size and the axis-ratio of the outer yield surface, $\alpha \in [0,1]$ and $\gamma \in [0,1]$ control the shape of the yield surface in the p-q plane, $\bar{\rho}(\theta)$ controls the deviatoric section and $R \in (0,1]$ is the ratio of the size of the inner and outer surfaces. From (**??**) it is apparent that introducing a cross-coupling in the rate of dissipation function results in the yield surface being sheared off the hydrostatic axis, where β_{ij} is a second order, traceless (deviatoric), tensor measure of this inclination. If $\beta_{ij} = 0$ we recover an isotropic yield surface, with the ellipsoid's major axis coincident with the hydrostatic axis.

The evolution of inelastic straining on the inner yield surface follows from the dissipation function and is controlled through

$$\frac{\dot{\varepsilon}^{\mathrm{p}}_{ij}}{\dot{\gamma}} = \frac{2}{3}\Big(B_f^2(p-p^\chi) - A_f^2 s^\beta_{ij}\beta_{ij}\Big)\delta_{ij} + 2A_f^2 s^\beta_{ij}. \qquad (7)$$

$\dot{\gamma}$ is the plastic consistency parameter (and not the rate of the material constant controlling the shape of the yield surface) that satisfies the Kuhn-Tucker-Karush consistency conditions: $\dot{\gamma} \geq 0$, $f \leq 0$ and $\dot{\gamma} f = 0$. Note, the position of isochoric flow on the yield surface depends on the level of anisotropy (loss CS uniqueness; see Section 3.1).

The ellipsoidal modified Cam clay (MCC) yield surface and associated flow direction is obtained by setting $\alpha = \gamma = 1$ and $R = 1$. Reducing α also causes an increase in the level of both plastic compaction and dilation through increasing the volumetric component of the plastic flow direction. Reducing γ has the opposite effect. There influence on the shape of the yield surface was detailed by **?**).

2.3 *Lode angle dependency*

The yield surface includes a dependency on the Lode angle, θ, through the normalised deviatoric yield radius, $\bar{\rho}(\theta)$, in B_f. Here, the model is presented with a Willam-Warnke (W-W) (**?**) LAD that can be expressed as

$$\bar{\rho}(\theta) = \frac{a_1 C + \sqrt{2a_1C^2 + a_2}}{2a_1C^2 + 1} \quad \in [\bar{\rho}_e, 1] \qquad (8)$$

where $a_1 = 2(1-\bar{\rho}_e^2)/(2\bar{\rho}_e - 1)^2$, $a_2 = (5\bar{\rho}_e^2 - 4\bar{\rho}_e)/(2\bar{\rho}_e - 1)^2$ and $C = \cos(\pi/6 - \theta)$. This W-W LAD is based on a local measure of the Lode angle, θ, from the major, β_{ij}, axis of the inner surface. This definition ensures convexity of the yield surface and in this case the Lode angle is calculated from

$$\theta = \frac{1}{3}\arcsin\left(\frac{-3\sqrt{3}}{2}\frac{J_3}{J_2^{3/2}}\right) \quad \in \big[-\pi/6, \pi/6\big], \qquad (9)$$

where $J_2 = \frac{1}{2}\big(r_{ij}r_{ji}\big)$, $J_3 = \frac{1}{3}\big(r_{ij}r_{jk}r_{ki}\big)$ and the normalised deviatoric distance from the inner surface axis of anisotropy is

$$r_{ij} = \frac{s_{ij} - s^\chi_{ij} + R p_c \gamma \beta_{ij}/2}{p - p^\chi + R p_c \gamma/2} \qquad (10)$$

Note that β_{ij} corresponds to a shearing of the yield surface in the deviatoric direction, rather than a rotation away from the hydrostatic axis. This distinction is important, as an initially convex yield surface will remain convex for any degree of shearing.

2.4 *Isotropic fluctuations*

The hydrostatic extent of both the inner and outer surfaces are controlled by p_c. The ratio of the size of the two surfaces is keep constant, specified by R. Here, following **?**), the rate of the evolution of the size of the outer surface is defined as

$$\dot{p_c} = \left(\frac{p_c}{\lambda - \kappa}\right)\dot{\varepsilon}^{\mathrm{p}}_v, \qquad (11)$$

where λ is the bi-logarithmic plastic compressibility index.

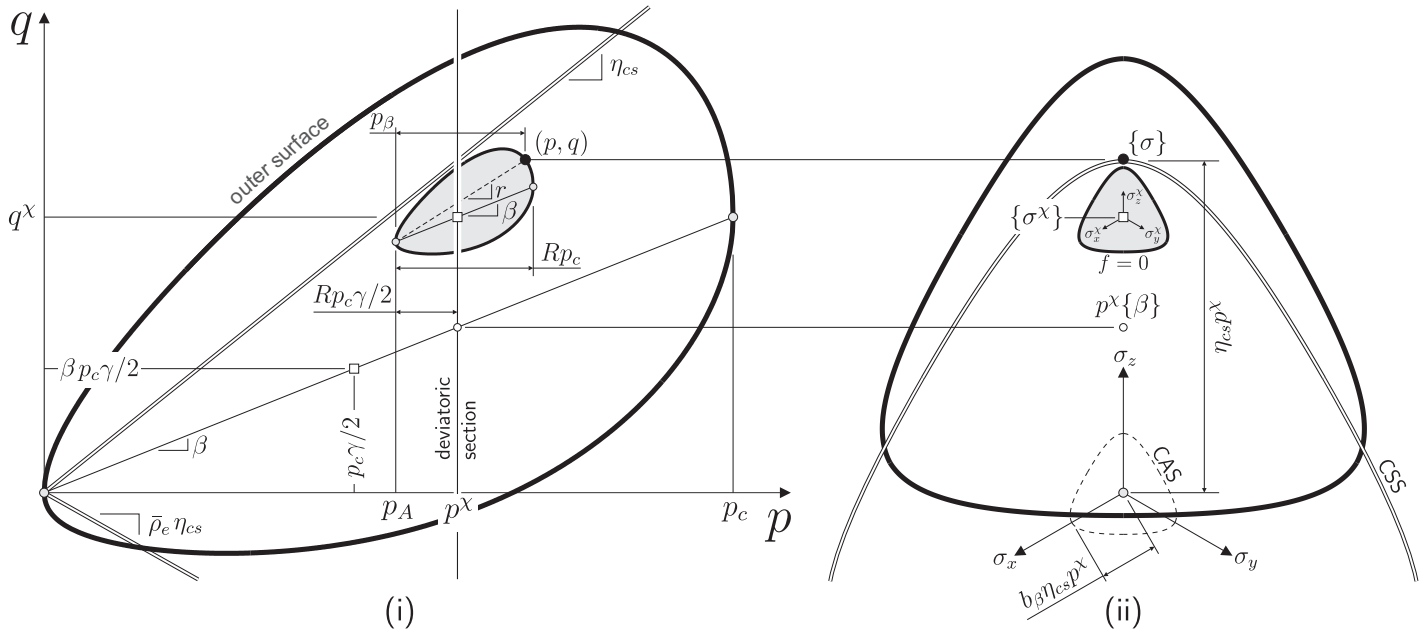

Figure 1: Two surface anisotropic model with $\eta_{cs} = 0.8$, $\alpha = 0.6$, $\gamma = 0.9$ and $\bar{\rho}_e = 0.7$: (i) in p-q stress space and (ii) deviatoric section through $p = p^\chi$. The LAD Critical State surface (CSS) and critical anisotropy surface (CAS) are identified in the deviatoric section. The current stress state is identified by a solid black circle whereas the centre of the yield surface is identified by a square.

2.5 *Anisotropic shearing*

The development of anisotropy, β_{ij}, in the two surface model is controlled through the following rate relationship by proposed by **?**) (based on the law developed by **?**))

$$\dot{\beta}_{ij} = C_\beta\Big(\big(r_{ij} - \beta_{ij}\big)\langle\dot{\varepsilon}^{\rm p}_v\rangle + x_\beta\big(b_\beta r_{ij} - \beta_{ij}\big)\dot{\varepsilon}^{\rm p}_\gamma\Big), \quad (12)$$

where $\langle(\cdot)\rangle$ is the ramp function of $(\cdot)$. Compressive volumetric plastic strains, $\dot{\varepsilon}^{\rm p}_v$, try to drag the level of anisotropy towards the local stress ratio, r_{ij}, whereas deviatoric plastic straining shifts β_{ij} in the direction of $b_\beta r_{ij}$, where b_β is a material constant. C_β controls the rate of anisotropic shearing and x_β the relative contribution of the volumetric and deviatoric strains on the development of anisotropy.

2.6 *Inner surface translation*

The movement of the inner surface is derived through the concept of a projection centre (**?**) and assuming that the outer *bounding* and inner *yield* surfaces are geometrically similar. The derivation of the law is omitted in this paper for brevity, it is simply given as

$$\begin{aligned}\dot{\sigma}^\chi_{ij} \;=\; & C_\chi||\dot{\varepsilon}^{\rm p}_{ij}||\Big((1-R)\sigma_{ij} + Rp_c\gamma\big(\delta_{ij}+\beta_{ij}\big)/2\Big) \\ & + \Big(\dot{\varepsilon}^{\rm p}_v/(\lambda-\kappa) - C_\chi||\dot{\varepsilon}^{\rm p}_{ij}||\Big)\sigma^\chi_{ij} + p^\chi\dot{\beta}_{ij}, \quad (13)\end{aligned}$$

where C_χ controls the rate of translation of the surface. This translation rule means that the inner yield surface can touch the outer surface but never overlap it. The rate of anisotropic shearing is scaled by the hydrostatic pressure at the centre of the inner surface to ensure that under plastic straining the centre of the surface translates appropriately, remaining consistent with the evolving anisotropy of the geometrically similar surfaces. The term involving purely volumetric plastic straining, $\dot{\varepsilon}^{\rm p}_v$, causes the yield surface centre to scale uniformly, from the origin, with isotropic expansion or contraction of the yield and outer envelopes. For full details of the derivation of the translation law see **?**), or **?**) for an abridged version.

2.7 *Complete formulation*

The two-surface anisotropic model is fully described by the equations in the preceding sub-sections. The model requires 12 constants: 2 associated with the hyperelasticity relationship, 6 with the isotropic envelopes and 4 with the development of anisotropy. These material constants are given in Table **??** for Lower Cromer Till and Sacramento river sand.

3 ASYMPTOTIC STATES

Unlike some anisotropic hardening laws, which depend purely on plastic volumetric strains (for example **?**) and **?**)), the expression adopted here gives rise to a unique level of anisotropy at the CS (provided that $x_\beta \neq 0$). This asymptotic of anisotropy is referred to here as the critical anisotropy state[1] (CAS). When approaching the CS the plastic volumetric strain diminishes while the level of anisotropy tends towards the deviatoric target value, $b_\beta r_{ij}$. In the limiting case, when $\dot{\varepsilon}^{\rm p}_v = 0$, the rate of evolution of anisotropy becomes

$$(\dot{\beta}_{ij})_{\dot{\varepsilon}^{\rm p}_v=0} = C_\beta x_\beta\big(b_\beta r_{ij} - \beta_{ij}\big)\dot{\varepsilon}^{\rm p}_\gamma. \quad (14)$$

[1]or critical anisotropy surface (CAS), as used in Figure **??**.

Under continued plastic shearing with no change in state, $\dot{\beta}_{ij} \to 0$ and $\beta_{ij}^{cs} = b_\beta r_{ij}^{cs}$, where $(\cdot)^{cs}$ denotes a quantity at the CS. The anisotropy of the yield surface when a material has reached the CS is independent of both (i) the initial anisotropy and (ii) the stress path taken to the reach this state. It is only dependent on the stress ratio at the CS and a material constant, b_β. This unique level of *fabric* anisotropy also results in a unique CSL in the bi-logarithmic void ratio versus hydrostatic pressure plane. The majority of previous formulations that include anisotropic shearing of the yield surface do not predict a unique CAS. One exception is the S-CLAY1 model (**?**), and subsequent extensions.

3.1 *Yield surface axis ratio*

It is important to distinquish between the material constant controlling the axis ratio of the yield surface, M, and the experimentally determined stress ratio at the CS (denoted here η_{cs} where $\eta = q/p$). If the model includes non-zero anisotropy at the CS (that is, if $b_\beta \neq 0$) then $M \neq \eta_{cs}$. Instead, M must be specified to obtain the correct stress ratio at the CS.

The position of isochoric plastic flow on the yield surface when at the CS is given by (**?**)

$$p^{cs} = \frac{1 - b_\beta + b_\beta\gamma(2-\gamma)}{b_\beta\gamma(2-\gamma) + \gamma(1-b_\beta)/2}, \tag{15}$$

where $p^{cs} = p_c/p$. Therefore the relative position of the CS on the outer surface is solely a function of b_β and γ. The value M required to obtain the correct η_{cs} is

$$M = \frac{\eta_{cs}(1 - \gamma + \gamma p^{cs}/2)(1 - b_\beta)}{(1 - \alpha + \alpha\gamma p^{cs}/2)\sqrt{\gamma(2-\gamma)(p^{cs}-1)}}. \tag{16}$$

In the case when $b_\beta = 0$ it is clear from the above equations that $p^{cs} = 2/\gamma$ and $M = \eta_{cs}$.

3.2 *The CS, K_0 loading & the friction angle*

Three of the material constants required for the two surface model are intimately linked to the effective friction angle, ϕ, those are: (i) the stress ratio at the CS, η_{cs}, (ii) the normalised deviatoric yield radius, $\bar{\rho}_e$, and (iii) constant controlling the relative contribution of the volumetric and deviatoric strains on the development of anisotropy, x_β.

The stress ratio at the CS is linked to ϕ through

$$\eta_{cs} = 2\sqrt{6}\sin\phi/\big(3 - \sin\phi\big) \tag{17}$$

and to the normalised deviatoric yield radius via

$$\bar{\rho}_e = (2 + k)/(2k + 1), \tag{18}$$

where $k = (1 + \sin\phi)/(1 - \sin\phi)$ is the passive earth pressure coefficient. x_β can be determined using the asymptotic stress ratio under K_0 loading, η_{K_0}, using

$$x_\beta = (\eta_{K_0} - \beta_{K_0})/\big(\sqrt{2/3}(\beta_{k_0} - b_\beta\eta_{K_0})\big), \tag{19}$$

constant		LCT	SRS
elastic compressibility	κ	0.005	0.0038
shear modulus (MPa)	G	28	40
yield surface axis ratio	M	0.92	0.96
plastic compressibility	λ	0.045	0.076
norm. dev. ext. yield	$\bar{\rho}_e$	0.73	0.68*
inner surface size ratio	R	0.2	0.2
shape constant	α	0.4	0.3
shape constant	γ	0.78	0.6
rate of anisotropy	C_β	14	6
stress path aniso.	x_β	4.8	7.0*
volumetric target	b_β	0.1	0.4
rate of translation	C_χ	2,000	4,000

Table 1: Material constants for Lower Cromer till (LCT) and Sacramento river sand (SRS). * denotes a constant determined from ϕ (taken as $34.6°$ for SRS).

where β_{K_0} is the level of anisotropy developed under continuous K_0 loading and can be obtained though the solution of a quartic equation involving γ, α, b_β, η_{cs} and η_{K_0} (see **?**) for details). If experimental data for η_{K_0} is not available, it can be estimated using the formula provided by **?**)

$$\eta_{K_0} = \sqrt{6}\sin\phi/\big(3 - 2\sin\phi\big). \tag{20}$$

This equation has been shown to provide reasonable agreement to measured data over a wide range of friction angles (**?**). Therefore obtaing η_{cs} from a single undrained traixal compression test, using the above equations, it is possible to determine ϕ and estimate $\bar{\rho}_e$ and x_β.

4 EXPERIMENTAL VALIDATION

This section presents the experimental validation of the model against data on both a clay (LCT) and a sand (SRS). The material constants for all of the numerical simulations are given in Tab;e **??**.

4.1 *Lower Cromer till (LCT)*

Figure **??** shows the experimental results from LCT (**?**) under undrained triaxial compression (UTC) and undrained triaxial extension (UTE) following one-dimensional (K_0) loading to a pressure of 233.3kPa (point B) and unloading to different (points B to G) over consolidation ratios (OCRs). The stress path response for the two-surface anisotropic model is shown in Figure **??** (i). The axial strain versus deviatoric stress response is shown in Figure **??** (ii). For all of the tests, the full stress path is simulated using a single set of material constants (as given in Table **??**). That is, the same constants are used for the complete response, including one-dimensional consolidation,

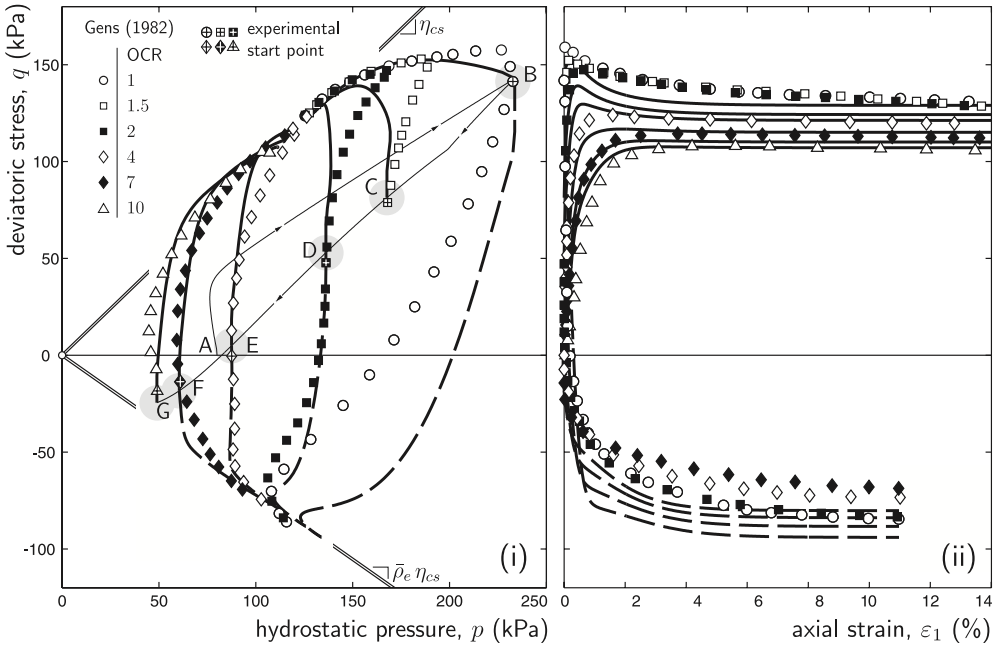

Figure 2: UTC and UTE tests following K0 consolidation and swelling comparison with experimental data (shown by discrete points) on LCT: (i) stress path in p-q space and (ii) axial strain-deviatoric stress response.

swelling and UTC or UTE. The two-surface model shows a reasonable agreement with the experimental data for all OCRs, as shown in Figure **??** (i) . The only significant deviation is under UTE at an OCR of 1, where an over-stiff response is observed.

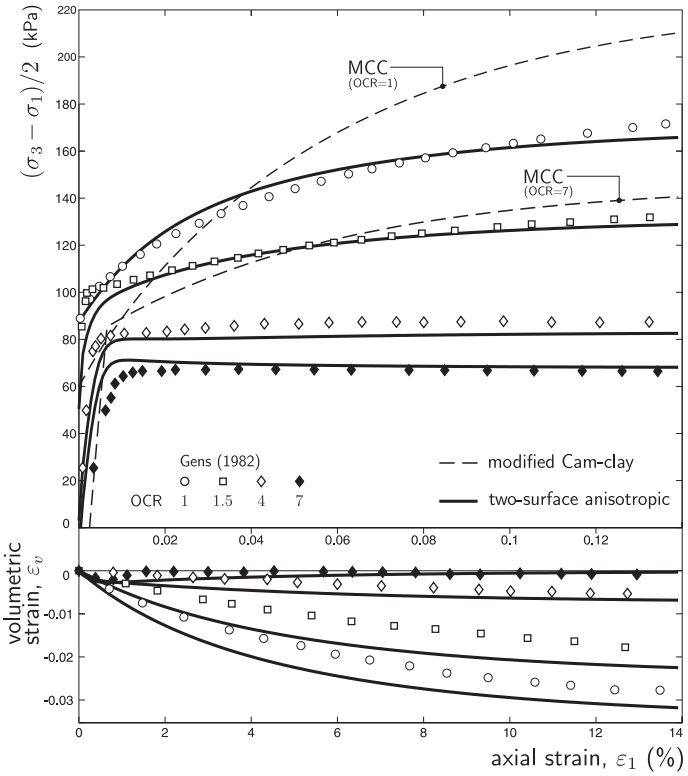

Figure 3: DTC tests following K0 consolidation and swelling comparison with experimental data (shown by discrete points) on LCT: axial strain-deviatoric stress response (above) and axial strain-volumetric strain response (below).

The experimental data and two-surface model responses under DTC following K_0 loading and unloading to five OCRs are shown in Figure **??** (along with the MCC model response for OCRs of one and seven shown by fine dashed lines). The two-surface model gives good agreement with the experimental data for all OCRs, in terms of both the principal stress deviation and the volumetric strain response. However, the MCC model significantly over-estimates the stress deviator for both the normally consolidated (OCR$=$ 1) and heavily over-consolidated (OCR$=$ 7) samples when compared with the experimental data.

4.2 *Sacramento river sand (SRS)*

Figure **??** shows the experimental results from dense SRS[2] (**?**, **?**) (with the data points obtained from **?**)) under UTC following hydrostatic compression to four different initial pressures. In order to account for this dense state, the two surface model was initially hydrostatically consolidated to a pressure of 6.2MPa (determined by assuming an initial void ratio of $e_{\text{in}} \approx 0.86$ for the loose sand) before unloading to the required pressure at the start of the UTC test. As with the tests on LCT, the full stress path is simulated using a single set of material constants (as given in Table **??**). The two surface model offers reasonable agreement for the four starting pressures in terms of both the p versus $(\sigma_1 - \sigma_3)$ and ε_1 versus $(\sigma_1 - \sigma_3)$ responses, as shown in Figures **??** (i) and (ii), respectively.

The experimental data on dense SRS (**?**, **?**) and two-surface model responses under DTC following hydrostatic loading and unloading to five different starting pressures are shown in Figure **??**. The two-surface model gives adequate overall agreement with the experimental data for all starting pressures, in terms of both the principal stress deviation and the volumetric strain response. However, the two surface model over predicts the level of volumetric dilation

[2]the sand had an initial void ratio of $e_{\text{in}} \approx 0.60$

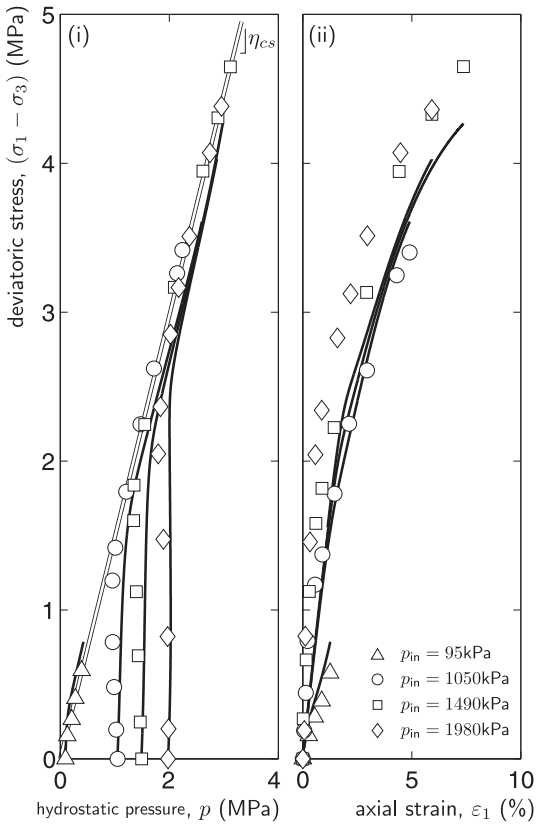

Figure 4: UTC tests at different starting pressures comparison with experimental data (shown by discrete points) on SRS: (i) stress path and (ii) axial strain-deviatoric stress response.

for the tests under a lower confining pressure.

5 OBSERVATIONS

This paper has distilled the key concepts behind a two-surface hyperplasticity model (**?**) whose development was informed by recent DEM findings on the uniqueness of the CS. Asymptotic states of the model are well defined and provide a useful means of calibration from classical relationships. Finally, the DEM-continuum-experimental loop was closed through comparison of the developed model with experimental data on both fine and coarse-grained particulate media. The simulations demonstrated, that providing the previous stress history is accounted for, the proposed model is suitable for a wide range of particulate media.

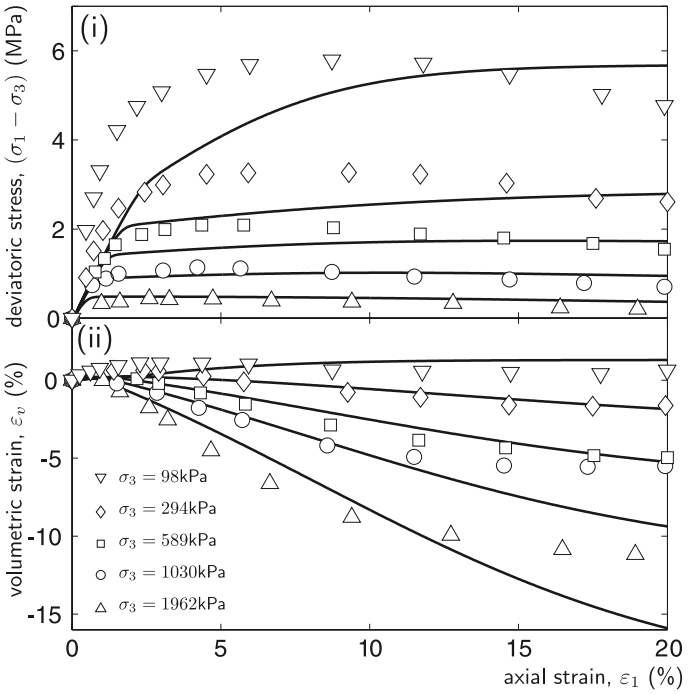

Figure 5: DTC tests at different starting pressures comparison with experimental data (discrete points) on SRS : (i) axial strain-deviatoric stress response and (ii) axial strain-volumetric strain response.